Density Reconstruction in Convergent High-Energy-Density Systems Using X-Ray Radiography and Bayesian Inference

S. Ressel,[1,*] J. J. Ruby,[1,2,†] G. W. Collins,[1,2,3] and J. R. Rygg[1,2,3]

[1]Laboratory for Laser Energetics, University of Rochester
[2]Department of Physics and Astronomy, University of Rochester
[3]Department of Mechanical Engineering, University of Rochester
[*]Currently at Department of Atmospheric Sciences, University of Washington
[†]Currently at Lawrence Livermore National Laboratory

X-ray radiography is a technique frequently used to diagnose convergent high-energy-density (HED) systems, such as inertial confinement fusion (ICF) implosions, and to provide unique information that is not available through self-emission measurements. We investigate the scope and limits of that information using a radiography simulation combined with Bayesian inference workflow. The accuracy of density reconstruction from simulated radiographs of spherical implosions driven with 20 kJ of laser energy is assessed, including the increase or decrease in accuracy due to the addition of Lagrangian marker layers, Poisson noise, and improved prior information. This work is the first to present the full uncertainty distributions inferred from radiography analysis in HED systems and demonstrates the importance of constructing the full posterior probability density, as opposed to a point estimate, due to the modal structure of the likelihood surface introduced by typical experimental noise sources. This general methodology can be used for both robust analysis of radiographic data and improved design of radiography experiments by modeling the full experimental system.

The inference workflow was tested on realistic data generated from the 1-D radiation-hydrodynamic code *LILAC*, where a single spherically converging shock wave was simulated in a solid hydrocarbon sphere (CH) driven by 27 kJ of UV light using the *SESAME* 7592 EOS table and Los Alamos's astrophysical opacity tables. The resulting radial density profiles are used to generate a simulated radiograph, using a straight-line ray trace to simulate the optical system of an x-ray streak camera with a slit imager, to determine how much density-profile information is encoded in the lineout and to what extent the density profile can be reconstructed from lineout data.

The parameterization used to represent the *LILAC* density profile is similar in form to previous work[1] and is given by

$$\rho(r) = \rho_0; r < r_s,$$

$$\rho(r) = \rho_s + (\rho_p - \rho_s)(r - r_s)/(r_p - r_s); r_s < r < r_p,$$

$$\rho(r) = \rho_p \cdot \exp\left[-(r - r_p)^2/(2\sigma^2)\right]; r_p < r < r_e,$$

$$\rho(r) = \rho_e \cdot \exp\left[-a(r - r_e)\right]; r_e < r,$$

$$\text{and } \sigma = \sqrt{-(r_p - r_e)^2/2\ln(\rho_e - \rho_p)}. \quad (1)$$

where r_s, r_p, and r_e are the radial locations of the shock, peak density, and tail, respectively; ρ_0, ρ_s, ρ_p, and ρ_e are the densities of the material in ambient conditions, immediately after being shocked, at its maximum due to converging flows, and at the tail of the density profile, respectively; and α is a scale parameter that determines how quickly the density reduces to zero in the tail.

The results of using Bayesian inference to construct the posterior probability densities for the parameters in the density profile (shown in Fig. 1) demonstrate that some additional information is needed to constrain the inferred shock compression. Figure 2(a) shows the uniform prior distribution (green) for the shock compression, alongside the posteriors from inference including an additional constraint and including noise. A defining feature of the inference from these cases is the upper limit placed on the shock compression, which can be used in combination with outside information to further constrain the posterior.

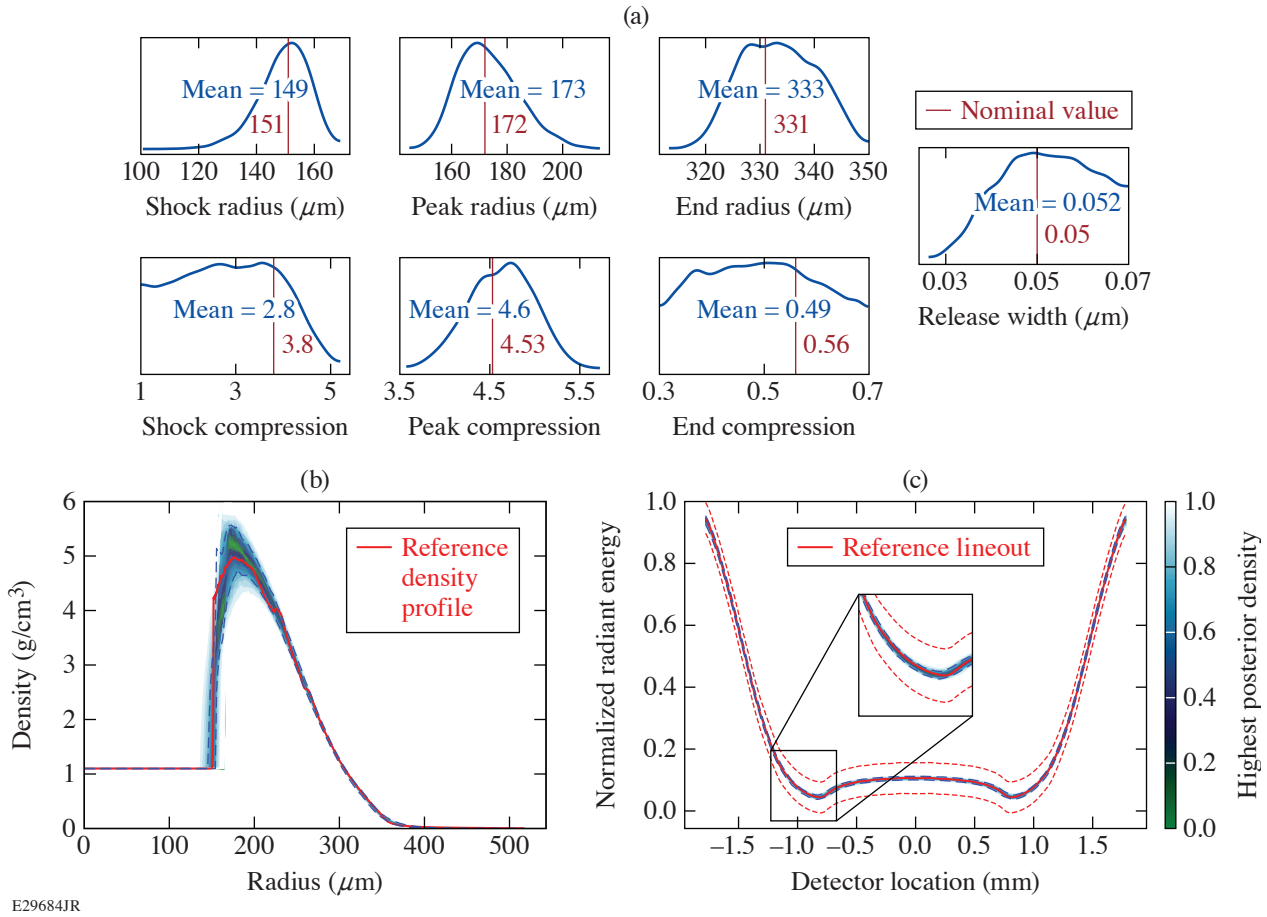

Figure 1

(a) Posterior distributions for each of the seven parameters of the model given in Eq. (1), as well as (b) posterior predictive distributions (PPD's) of the density profiles and (c) lineouts generated from said posterior distributions. A number of the parameters are well constrained, as shown by a single narrow peak in their posterior distributions, including the location of the shock, the location of the peak density, and the peak compression, and they all recover the underlying nominal value, given by the vertical red line, which is the least-squares best fit value recovered by fitting the simulated density profile with the assumed model. Notably, the posterior distribution for the shock compression (ρ_s/ρ_0) is not well constrained, presenting an upper bound of about 4, but roughly equal probability density across all values below 4. This can also be seen in (b), which is well matched to the reference density profile outside the region of the shock. Despite this, the PPD's of the lineouts in (c) are converged from the inference and well matched to the reference information, even around the feature due to the shock limb highlighted in the inset.

The simplest way to introduce this outside information is by using a more-informed prior distribution—for example, one that introduces a lower limit on the shock compression. A naive implementation is shown in Fig. 2(b) where the data-informed prior (orange) is simply a uniform distribution with a lower bound set by the maximum compression measurement of 3.39 (Ref. 2)

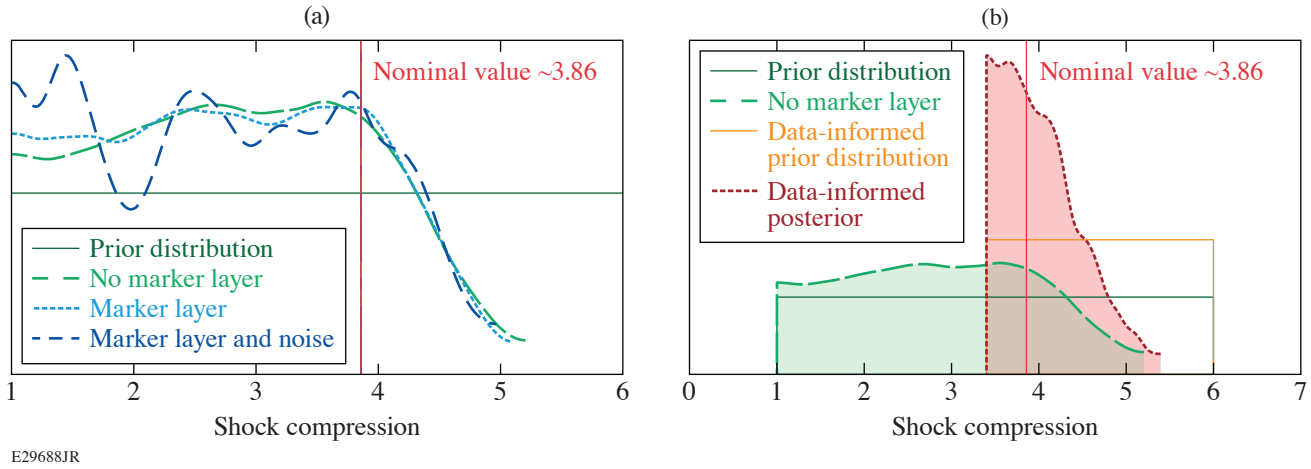

Figure 2

(a) Posterior distributions of the shock compression (ρ_s/ρ_0) for the cases with no noise and no Lagrangian marker layer (dashed green curve), no noise with a Lagrangian marker layer (dotted light blue curve), and with noise and a Lagrangian marker layer (dashed dark blue curve). Also shown are the prior used for each case (solid green, horizontal line) and the nominal value from the *LILAC* density profile (solid red, vertical line), given as ~3.86. All of the distributions show the same general trend that above a compression of 4 the probability density drops sharply, due to the peak compression behind the shock being well constrained and the shock jump necessarily being smaller, effectively giving an upper bound on the shock jump. There is little constraint on the lower end of the compression where the probability density is effectively flat between 1 and 4. The case with noise shows modal structure that, if point estimates are used, can give the impression of constraint while being only a local maximum in probability density. (b) The posterior for shock compression (dashed green curve) for the case with a broad uniform prior (solid green line) and posterior (dotted red curve) for the case with a narrow uniform prior (solid orange line) truncated at the low end at the location of previous measurements.[2] This demonstrates how Bayesian inference allows additional information to be leveraged to constrain a quantity that is otherwise unconstrained. The combination of the prior informing a lower limit of compression and the radiograph constraining upper limits of compression results in a nicely peaked posterior probability density that captures the proper underlying value (solid red line). The axes are expanded to demonstrate how the priors enforce that there is zero probability density outside of their bounds. Note that the data-informed posterior is largely asymmetric, although it presents a strongly peaked result that recovers the nominal value.

from previous data along the Hugoniot of CH up to 8.74 Mbar performed in planar geometry using a different methodology. Figure 2(b) also shows the posterior for shock compression given the new prior (red), which is now significantly more peaked than the previous results (green), meaning that there is a well-defined region of high probability density.

Although the shock compression is not strongly constrained by the radiograph alone, the density profile is well constrained by the radiograph measurement. In particular, the areal density (ρR) is very well constrained and is a quantity of particular interest within the ICF community. The findings here are in excellent agreement with previous radiography measurements taken on shells for the purpose of diagnosing metrics relevant to ICF modeling.[3] This work can be seen as an extension of those efforts with additional insight into the uncertainties associated with such reconstructions. Additionally, the peak density achieved within the bulk of the material behind the shock, which has a great effect on the propagation of the outgoing shock wave, is well constrained. Radiography measurements of this kind contain a great deal of information that can be used in combination with other measurements to develop a full picture of implosion experiments, including how materials respond to strong converging shock waves. This work can be used as a foundation to develop further investigations about the information contained in measurements of this type.

This material is based upon work supported by the Department of Energy National Nuclear Security Administration under Award Number DE-NA0003856, the U.S. Department of Energy, Office of Science, Office of Fusion Energy Sciences under Award No. DE-SC001926, the University of Rochester, and the New York State Energy Research and Development Authority.

1. D. C. Swift *et al.*, Rev. Sci. Instrum. **89**, 053505 (2018).
2. M. A. Barrios *et al.*, Phys. Plasmas **17**, 056307 (2010).
3. D. G. Hicks *et al.*, Phys. Plasmas **17**, 102703 (2010).